Acta Cryst. (1951). **4**, 1

Effect of Crystal, Grain, and Particle Size on X-ray Power Diffracted from Powders*

BY ZIGMOND W. WILCHINSKY†

Esso Laboratories, Esso Standard Oil Company, Baton Rouge, Louisiana, U.S.A.

(*Received* 22 *July* 1949 *and in revised form* 2 *April* 1950)

A theoretical and experimental investigation has been made on diffraction of X-rays from crystalline powders in which the diffracted power is modified by the powder coarseness and absorption inhomogeneities in the sample. Compared with previous theories, the present theory is more extensive and has been found to fit the experimental data better. The magnitude of the diffracted power is related theoretically to particle diameter, linear absorption coefficient, degree of compaction of the powder, crystal size, primary extinction coefficient, crystal-chemical composition and grain size for polyphased particles. It is shown theoretically and experimentally that these variables can cause the diffracted power to be significantly different from that for an ideal case. For a powder of a single substance (iron), excellent agreement between theory and experiment has been obtained for the effects due to particle size, absorption coefficient and degree of compaction. Theoretical predictions of diffracted power from an iron-tungsten mixture have been substantiated experimentally. Measurements on heat-treated iron samples show that the diffracted power decreases with increasing crystal size, and indicate that the equation for this effect might be useful in determining crystal sizes in the range 10^{-5} to 10^{-3} cm.

Introduction

It has been pointed out by a number of investigators that integrated intensities in powder X-ray diffraction patterns can be modified by the state of subdivision of the sample material. Illustrations of these effects due to crystal and particle size are shown in the X-ray spectrometer traces (Figs. 1 and 2). The decrease in diffracted power for the heat-treated samples (Fig. 1) can be explained qualitatively on the basis that the crystals have grown large enough for primary extinction (Darwin, 1914; Compton & Allison, 1946, chap. 6) to become noticeable, and that this effect is more prominent with increasing crystal size resulting from increasing severity of heat treatment. In Fig. 2 the integrated intensities are smaller for the coarser powders than for the fine powder or the solid block. This behavior can be qualitatively explained by the entrapment of X-rays in the crevices between the particles as illustrated in Fig. 3. An exact general theory to account quantitatively for these and related effects has not been set forth, primarily because of the inherent complexity of the problem. On the other hand, theories of too limited scope have proved to be generally unsatisfactory and have resulted in placing the problem in a somewhat controversial status. In one of his papers, Brindley (1945), after critically reviewing the works of Rusterholz (1931), Schäfer (1933), Brentano (1935, 1938), and Taylor (1944*a*, *b*), concludes that there is lack of agreement on several aspects of the problem and proceeds to develop a new theory for the diffraction

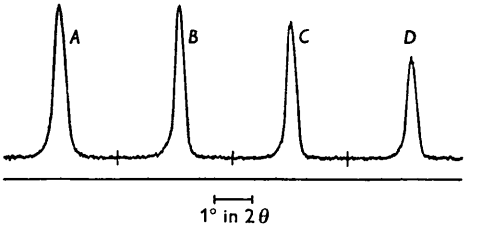

Fig. 1. X-ray spectrometer traces of the (110) line of iron, illustrating the effect of crystal size on diffracted power. Trace *A* is for a sample of material *B* in Table 1. Other traces are for the same sample material, treated to induce crystal growth by the following heat treatments: 80 min. at 900° F. for trace *B*, 15 min. at 1500° F. for *C*, and 2 hr. at 1500° F. for *D*. X-ray wave-length = 1·93 A.

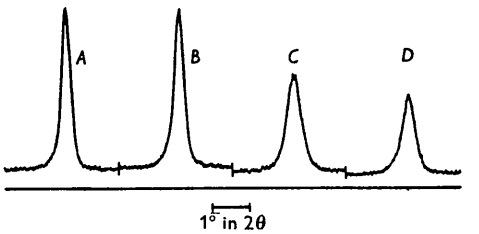

Fig. 2. X-ray spectrometer traces of the (110) line of iron, illustrating effects of powder coarseness and degree of compaction on diffracted power. Trace *A* is for a fine powder (*B* in Table 1), *B* is for a solid Armco iron block, traces *C* and *D* are respectively for coarse and very coarse sawdust of Armco iron (sample materials *H* and *J* in Table 1). X-ray wave-length = 1·93 A.

of X-rays from coarse powders. More recently de Wolff (1947) pointed out that Brindley had made an

* Presented at the First Congress of the International Union of Crystallography, 28 July 1948, at Harvard University, Cambridge, Massachusetts, U.S.A.

† Present Address: Esso Laboratories, Standard Oil Development Company, Linden, New Jersey, U.S.A.

unjustified over-simplification which constitutes a weak point in his treatment of the problem. Although the physical considerations in de Wolff's approach to the problem are sound, the complexity of his mathematical development makes his theory rather difficult to apply. In the present paper, a more comprehensive development, including several new facets of the problem, is formulated by means of a simplified theoretical approach. Also, results of a number of experiments devised to test the validity of this and other theories are presented.

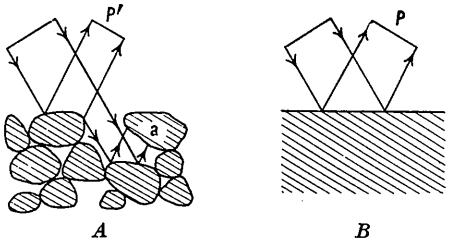

Fig. 3. A qualitative demonstration of the decrease in diffracted power due to powder coarseness. In A, part of the diffracted beam is absorbed by particle a so that the measured diffracted power P' is less than the power P measured for the ideal powder in sketch B.

Theory for a powder of a single substance

Let the term *ideal powder* designate a powder with the following characteristics: (1) the crystals are small enough so that the effect of primary extinction is negligible; and (2) the particle size is sufficiently small so that the powder can be considered homogeneous with respect to applying the simple law of absorption of X-rays in the sample. For a given Bragg reflection, the power diffracted from a non-ideal powder will be compared with that from a similar sample of ideal powder. These power ratios are obtained experimentally as ratios of integrated intensities.

For a plane sample in the conventional spectrometer arrangement (Friedman, 1945), the integrated intensity, P_0, for an ideal powder of a single substance can be easily obtained with reference to Fig. 4. Let A be the cross-section area of the X-ray beam and dx the thickness of an elemental slab. The elemental volume dV is then $(A/\sin\theta)\,dx$ and the contribution to the integrated intensity corresponding to the Bragg angle θ is

$$dP_0 = vIQ\{\exp(-2v\mu x/\sin\theta)\}(A/\sin\theta)\,dx, \qquad (1)$$

where I is the average intensity of the incident beam over the cross-sectional area, Q is the integrated intensity per unit volume of solid material (not including absorption) per unit intensity of primary beam, μ is the linear absorption coefficient of the solid material, and v is the fraction of the volume occupied by solid material. Unless otherwise stated, it will be assumed that no binder is employed, so that $(1-v)$ is the fractional volume occupied by voids. For a sample thick enough to be considered opaque, the value P_0 is obtained by integrating the right-hand side of (1) between the limits zero and infinity, the result being

$$P_0 = AIQ/(2\mu). \qquad (2)$$

For a non-ideal sample, let us first consider the laminar model in Fig. 5. The particles of thickness $Y\sin\theta$ are subdivided into crystal plates of thickness $T\sin\theta$, and the lengths and breadths of the particles and crystals are large compared with Y and T, respectively. Also the particles and crystal have random sizes, shapes and orientations, within the limits allowed by the foregoing restrictions. For this geometry, which differs somewhat from Schäfer's cubical arrangement (Schäfer, 1933), a rather rigorous treatment can be given. With slight modification, the equations developed for this hypothetical case become approximate solutions for other shapes.

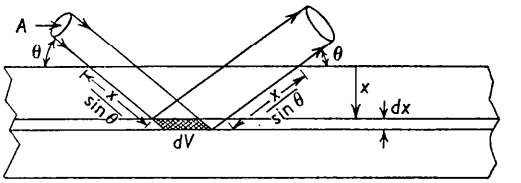

Fig. 4. Diffraction of X-rays from a flat powder block in a symmetrical position.

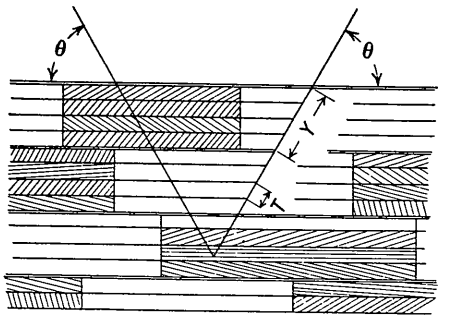

Fig. 5. Laminar model, in which flat particles of thickness $Y\sin\theta$ are further subdivided into crystal laminae of thickness $T\sin\theta$.

In a crystal layer of this laminar model, two types of crystals must be considered—reflecting and non-reflecting. Owing to the phenomenon of primary extinction in the reflecting crystals, the attenuation of the incident and reflected beams is greater in these regions than in the non-reflecting crystals which obey the ordinary absorption law. Let p be the integrated intensity for a crystal layer considered by itself. The average diffraction for an elemental slab dx can then be written

$$dp = vIQ\{\exp(-2\epsilon x/\sin\theta)\}(A/\sin\theta)\,dx, \qquad (3)$$

where ϵ is an effective *attenuation coefficient* which can be considered as the sum of the ordinary absorption coefficient and a term due to primary extinction. In-

tegration of (3) between the limits $x=0$ and $x=T\sin\theta$ gives

$$p=vP_0\frac{\mu}{\epsilon}\{1-\exp(-2\epsilon T)\}, \tag{4}$$

the group IQA having been eliminated by (2).

Let P_{mn} be the contribution to the integrated intensity from the mth crystal layer located in the nth particle layer of the sample. Then

$P_{mn}=p\times$(absorption factor due to the $(m-1)$ overlying crystal layers within the particle layer)$\times$ (absorption factor due to $(n-1)$ overlying particle layers). (5)

Hence, the integrated intensity, P, for an opaque sample is

$$P=\sum_{n=1}^{\infty}\sum_{m=1}^{M}P_{mn}, \tag{6}$$

where M is the number of crystal layers in a particle layer.

In determining the absorption due to $(m-1)$ crystal layers above the reference layer, the effect of *secondary extinction* can be considered negligible (Compton & Allison, 1946, chap. 6; Havinghurst, 1926). Hence, using the ordinary absorption law, the absorption factor for the $(m-1)$ overlying crystal layers is

$$\exp\{-2(m-1)\mu T\}. \tag{7}$$

Finally, the absorption factor for the $(n-1)$ particle layers can be obtained in a statistical manner. In traversing one particle layer at a grazing angle of incidence θ, the beam is attenuated by the factor

$$v\exp(-\mu Y)+v_0, \tag{8}$$

where $v_0=1-v$ is the fraction of the volume occupied by voids. In general, the absorption path of a diffracted ray is independent of that for the associated incident ray so that the absorption factor for a single overlying layer due to the two traversals involved is

$$\{v\exp(-\mu Y)+v_0\}^2, \tag{9}$$

and for $(n-1)$ layers the required absorption factor is

$$\{v\exp(-\mu Y)+v_0\}^{2(n-1)}. \tag{10}$$

However, in the case of exact back reflection ($\theta=90°$), the paths of the incident and diffracted rays are coincident, leading to the adsorption factor

$$\{v\exp(-2\mu Y)+v_0\}^{n-1} \tag{11}$$

for $(n-1)$ overlying particle layers, the quantity within the bracket being the absorption factor for the incident and diffracted rays for a single layer. Although diffraction very close to $\theta=90°$ is rarely realized in practice, a consideration of the integrated intensity at this limit can be made with very little additional effort and will result in a more complete treatment of the problem.

The values given by (4), (7) and (10), along with the additional relationship $MT=Y$, upon being inserted into (5) and (6) lead to the expression

$$\begin{aligned}\frac{P}{P_0}&=\frac{\mu}{\epsilon}\{1-\exp(-2\epsilon T)\}\times\sum_{m=1}^{M}\exp\{-2(m-1)\mu T\}\\&\quad\times\sum_{n=1}^{\infty}\{v\exp(-\mu Y)+v_0\}^{2(n-1)}\\&=\left[\frac{\mu}{\epsilon}\frac{1-\exp(-2\epsilon T)}{1-\exp(-2\mu T)}\right]\left[\frac{1+\exp(-\mu Y)}{2-v\{1-\exp(-\mu Y)\}}\right].\end{aligned} \tag{12}$$

It can be easily verified that this equation is in agreement with the diffraction behavior illustrated in Figs. 1 and 2, i.e. the integrated intensity decreases with increasing crystal and particle sizes, and the diffraction from a solid block is equivalent to that from a fine powder, each having the same crystal size. Also, equation (12) is consistent with the definition of an ideal powder in that $P\to P_0$ as $T\to 0$ and $Y\to 0$.

Before discussing the theoretical results more quantitatively, application of (12) to actual powders will be considered. For convenience, the first square bracket in (12), associated with the crystal size, will be referred to as the *crystal factor*; similarly, the second square bracket will be referred to as the *particle factor*. Let us first consider the effect of particle size in an actual sample consisting of particles having a measured diameter D. In diffracting from a subsurface particle, the incident and diffracted rays pass through regions of solid material and voids arranged in a somewhat random manner. This condition is similar to that in the laminar model and would lead one to expect a particle factor to be operative. Provided that this particle factor does not exceed the lower limit given by that for the laminar model having the same value of v, there is a value of Y in (12) which corresponds to D in the actual sample. The problem then reduces to finding a relationship between Y and D.

To a first approximation $Y=\frac{2}{3}D$ based on the fact that the average path length through a sphere is two-thirds the diameter. A more accurate relationship can be expressed

$$Y=\tfrac{2}{3}D(1+\alpha), \tag{13}$$

where α is a constant that can be determined experimentally. Similarly, in considering the crystal factor, the transformation to actual samples can be made through the relation

$$T=\tfrac{2}{3}L(1+\beta), \tag{14}$$

where L is the measured crystal diameter and β is an empirical corrective term. Thus, for a sample of a single substance consisting of particles of diameter D and crystals of diameter L,

$$\begin{aligned}\frac{P}{P_0}&=\left[\frac{\mu}{\epsilon}\frac{1-\exp\{-\frac{4}{3}\epsilon L(1+\beta)\}}{1-\exp\{-\frac{4}{3}\mu L(1+\beta)\}}\right]\\&\quad\times\left[\frac{1+\exp\{-\frac{2}{3}\mu D(1+\alpha)\}}{2-v(1-\exp\{-\frac{2}{3}\mu D(1+\alpha)\})}\right].\end{aligned} \tag{15}$$

The curves in Figs. 6 and 7 illustrate the behavior of (15) with respect to the various parameters. Denoting by subscripts the algebraic conditions imposed on (15), the particle factor can be designated $(P/P_0)_{L\to 0}$ and the crystal factor $(P/P_0)_{D\to 0}$. In Fig. 6, $(P/P_0)_{L\to 0}$ is plotted versus $\mu D(1+\alpha)$ for various values of v. In general, $(P/P_0)_{L\to 0}$ decreases with increasing $\mu D(1+\alpha)$ and decreasing v; however, limiting minimum values are obtained for each value of either of these parameters. The lowest value of $(P/P_0)_{L\to 0}$ is 0·5, occurring for a very loosely packed coarse powder.

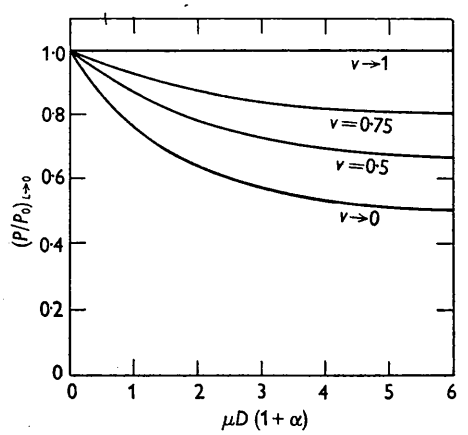

Fig. 6. Dependence of diffracted power on particle size and absorption coefficient for various degrees of compaction in a powder of a single substance.

The crystal factor could probably be discussed most effectively in terms of specific cases. For this purpose it is necessary to have values of ϵ. These can be approximated by

$$\epsilon=\mu_e+\mu, \tag{16}$$

where μ_e is Darwin's approximation (Darwin, 1914) for the *primary extinction coefficient*. The presence of μ in (16) is justified on the basis that in the derivation of μ_e, the ordinary absorption coefficient had been left out of consideration in order to simplify the mathematical development. The equation for evaluating μ_e is

$$\mu_e=\frac{3\pi}{16}\lambda FN\frac{e^2}{mc^2}\frac{1+\cos^2 2\theta}{1+\cos 2\theta}, \tag{17}$$

where λ is the X-ray wave-length, F the structure factor, N the number of unit cells per unit volume, e the electronic charge in electrostatic units, m the electronic mass, and c the speed of light. For purposes of this discussion the values of ϵ given by (16) will be considered sufficiently accurate.*

In Fig. 7 the crystal factor is shown plotted against $\mu L(1+\beta)$ for the following values of ϵ/μ: 2·8 for tungsten diffracting Fe $K\alpha$ radiation from the (110) planes; 8·0 for iron, Fe $K\alpha$ radiation, (110) planes; and 70·5 for calcite, Mo $K\alpha$ radiation, (100) planes. It can be seen in this figure that for a given $\mu L(1+\beta)$ the crystal factor decreases with increasing ϵ/μ. A serious departure from the ideal value can occur even for crystals that do not ordinarily show 'speckling' in a powder pattern. For instance, the curves indicate that a 20 % decrease in integrated intensity occurs for crystal of approximately $3{\cdot}3\times10^{-5}$, $8{\cdot}7\times10^{-5}$ and 19×10^{-5} cm. for the tungsten, iron and calcite respectively.

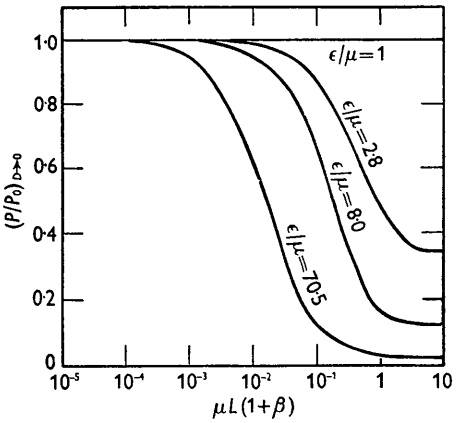

Fig. 7. Diffracted power as a function of crystal size, absorption coefficient, and ϵ/μ.

In deriving the non-ideal powder diffraction equation for the special case of $\theta=90°$, equation (11) must be used instead of (10) for the absorption factor due to $(n-1)$ overlying particle layers. Carrying the development through the transformation to an actual sample, one obtains

$$\left(\frac{P}{P_0}\right)_{\theta=90°}=\frac{\mu}{\epsilon}\frac{1-\exp\{-\frac{4}{3}\epsilon L(1+\beta)\}}{1-\exp\{-\frac{4}{3}\mu L(1+\beta)\}}. \tag{18}$$

It is interesting to note that (18) is independent of particle size, but consists only of a crystal factor identical to that in (15).

For samples prepared with a binder, the absorption due to binder material can usually be taken into account. If the space between the particles is completely filled with a binder of linear absorption coefficient μ_b, then v_0 in (8) should be replaced by $v_b\exp(-\mu_b Y)$, where v_b is the fractional volume occupied by the binder. Making this change leads to the result

$$\frac{P}{P_0}=\frac{\mu}{\epsilon}\frac{1-\exp\{-\frac{4}{3}\epsilon L(1+\beta)\}}{1-\exp\{-\frac{4}{3}\mu L(1+\beta)\}} \times\frac{v(1-\exp\{-\frac{4}{3}\mu D(1+\alpha)\})}{1-[v\exp\{-\frac{2}{3}\mu D(1+\alpha)\}+v_b\exp\{-\frac{2}{3}\mu_b D(1+\alpha)\}]^2}. \tag{19}$$

Theory for mixed powder

The theory can be extended to powders of two or more components by following the same general procedure as was used for a single substance. In the laminar

* Using available data, equation (16) was applied to the case of a single crystal of calcite. Letting ϵ' be the exact value of the desired attenuation coefficient according to Prins' (1930) refined theory which takes ordinary absorption into account, the ratio ϵ/ϵ' was computed to be 1·03 for $\lambda=0{\cdot}71$ A., 1·08 for $\lambda=1{\cdot}54$ A., and 1·03 for $\lambda=2{\cdot}29$ A., the last ratio being evaluated for a wavelength near the K critical absorption edge of calcium.

model, let a particle be built up of *grains*, each grain containing only one component. In turn, the grains are built up of crystals. Denoting quantities pertaining to the ith component by the subscript i, the contribution to P_i from the mth crystal layer located in the gth grain layer in the nth particle layer is

$$P_{ingm}=p_i\times(\text{absorption factor for the } (m-1) \text{ overlying crystal layers in the grain of the } i\text{th component})\times(\text{absorption factor for } (g-1) \text{ overlying grain layers in the particle})\times(\text{absorption factor for } (n-1) \text{ particle layers}). \quad (20)$$

The integrated intensity for a line of the ith component is then

$$P_i=\sum_{n=1}^{\infty}\sum_{g=1}^{G}\sum_{m=1}^{M}P_{ingm}, \quad (21)$$

where G is the number of grain layers in a particle. The values of the factors in (20), in terms of the laminar model, are

$$p_i=P_{0i}v_i\frac{\mu_i}{\epsilon_i}\{1-\exp(-2\epsilon_i T_i)\}, \quad (22)$$

absorption factor for $(m-1)$ crystal layers

$$=\exp\{-2(m-1)\mu_i T_i\}, \quad (23)$$

absorption factor for $(g-1)$ grain layers

$$=\left\{\sum_j\frac{v_j}{v}\exp(-\mu_j S)\right\}^{2(g-1)}, \quad (24)$$

absorption factor for $(n-1)$ particle layers

$$=\left\{v\left[\sum_j\frac{v_j}{v}\exp(-\mu_j S)\right]^G+v_0\right\}^{2(n-1)}, \quad (25)$$

where P_{0i} is the integrated intensity for an ideal powder of only the ith component, $S\sin\theta$ is the thickness of a grain layer and v_j is the volume fraction of the sample occupied by the jth component. Using these values in (20), the summation in (21) can be easily carried out. The integrated intensity for the laminar model thus obtained can be applied to typical powders by the general procedure employed for a single substance. Letting

$$S=\tfrac{2}{3}Z(1+\gamma), \quad (26)$$

where Z is the grain diameter and γ is a corrective term, the equation for the integrated intensity for the ith component can be expressed

$$\frac{P_i}{P_{0i}}=\left[\frac{v_i\mu_i}{\bar{\mu}}\right]\left[\frac{\mu_i}{\epsilon_i}\frac{1-\exp\{-\frac{4}{3}\epsilon_i L_i(1+\beta_i)\}}{1-\exp\{-\frac{4}{3}\mu_i L_i(1+\beta_i)\}}\right]\times\left[\frac{\bar{\mu}}{v\mu_i}\frac{1-\exp\{-\frac{4}{3}\mu_i Z(1+\gamma)\}}{1-\left(\sum_j\frac{v_j}{v}\exp\{-\frac{2}{3}\mu_j Z(1+\gamma)\}\right)^2}\right]\times\left[v\frac{1-\left(\sum_j\frac{v_j}{v}\exp\left\{-\frac{2}{3}\mu_j\frac{D}{G}(1+\gamma)\right\}\right)^{2G}}{1-\left\{v\left(\sum_j\frac{v_j}{v}\exp\left\{-\frac{2}{3}\mu_j\frac{D}{G}(1+\gamma)\right\}\right)^G+v_0\right\}^2}\right], \quad (27)$$

where $\bar{\mu}=\sum_j v_j\mu_j$ is the average linear absorption coefficient for the sample. In the form written, (27) has a simple physical interpretation in terms of the four main factors. The first square bracket is the value of P_i/P_{0i} for an ideal mixed powder. The second bracket can be recognized as a crystal factor of the same form as in (15). The third square bracket is a *grain factor* whose value approaches unity as the grain size approaches zero. The last square bracket is a particle factor, dependent to some extent on the grain size. As the grain size approaches zero, this factor assumes the same form as the particle factor for a single substance. Hence, for an ideal powder (D, Z and $L\to 0$), equation (27) reduces to the first factor.

The behavior of (27) is illustrated in Figs. 8–11 for an iron–tungsten system diffracting Fe $K\alpha$ X-radiation. The values $\alpha=\beta=\gamma=0$ were used in all these curves. In Fig. 8, the effect of crystal size in the binary mixture is shown for small particle and grain sizes. The curves for $L\to 0$ represent the values for an ideal powder. Since the crystal factor for any component is independent of the other components, any curve for tungsten in Fig. 8 can be considered with any of the curves for iron. The effects of particle size, grain size and degree of compaction are illustrated in Figs. 9, 10 and 11 respectively. In these figures, the grain and particle sizes for iron are the same as those for tungsten, hence the curves should be considered in associated pairs. This assortment of examples serves to illustrate the large modifications in integrated intensities that can arise from the state of subdivision of the materials in a mixture.

For the special case of $\theta=90°$, the integrated intensity for a component in the mixture is

$$\left(\frac{P_i}{P_{0i}}\right)_{\theta=90°}=\left[\frac{v_i\mu_i}{\bar{\mu}}\right]\left[\frac{\mu_i}{\epsilon_i}\frac{1-\exp\{-\frac{4}{3}\epsilon_i L_i(1+\beta_i)\}}{1-\exp\{-\frac{4}{3}\mu_i L_i(1+\beta_i)\}}\right]\times\left[\frac{\bar{\mu}}{v\mu_i}\frac{1-\exp\{-\frac{4}{3}\mu_i Z(1+\gamma)\}}{1-\sum_j\frac{v_j}{v}\exp\{-\frac{4}{3}\mu_j Z(1+\gamma)\}}\right]\times\left[v\frac{1-\left[\sum_j\frac{v_j}{v}\exp\left\{-\frac{4}{3}\mu_i\frac{D}{G}(1+\alpha)\right\}\right]^G}{1-\left[v\left(\sum_j\frac{v_j}{v}\exp\left\{-\frac{4}{3}\mu_j\frac{D}{G}(1+\alpha)\right\}\right)^G+v_0\right]}\right] \quad (28)$$

In contrast with equation (18) for a single substance, equation (28) for a mixed powder is not independent of particle size, except for $Z\to 0$, i.e. $G\to\infty$.

Comparison of experiment with theory

Experiments to test the theoretical equations for the effects of particle size, degree of compaction, and crystal size, in a powder consisting of a single substance, were carried out on specially prepared samples of iron powder. For the case of mixed powders, a tungsten–iron

mixture was used to test the particle-size effect. These experiments will be discussed in some detail after a few preliminary remarks are made about the general experimental procedure.

Integrated intensity values were measured for flat rotating samples with a Norelco Geiger counter X-ray spectrometer using an iron-target tube. The (110) line of iron (or tungsten) was scanned at the rate of 0·25° in 2θ per min. Then P is proportional to the total

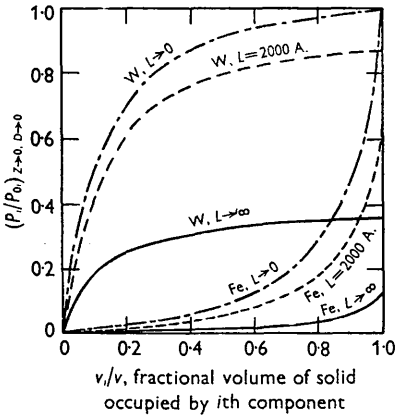

Fig. 8. Effect of crystal size on power diffracted from a binary mixture of iron and tungsten. Curves are for the (110) reflections, Fe $K\alpha$ radiation.

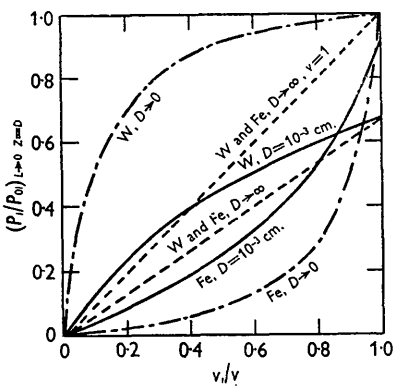

Fig. 9. Effect of particle size on power diffracted from an iron–tungsten mixture. Both components have the same particle size, and $v=0{\cdot}5$ except where indicated otherwise. Fe $K\alpha$ radiation is considered.

number of quanta counted during the scan, minus the background count. For a powder of a single substance consisting of fine particles, and crystals smaller than 1000 A., the probable error in precision for a single measurement of P was found to be less than $\pm 0{\cdot}01P$. In most cases, two or more power measurements were made for each sample. The number of determinations were generally too few for formal statistical treatment; however, the precision can be judged from the fact that the deviations (regardless of sign) from the mean were less than $0{\cdot}03P$ in all cases and less than $0{\cdot}01P$ for the majority of the cases. The precision in determining P/P_0 is thus sufficient for detecting the predicted effects.

Samples used for investigating the effect of particle size in a single substance and in a mixture were prepared with a very small amount of binder. The fraction of the radiation absorbed by the binder between the particles was estimated to be very slight—of the order of 0·001. A reliable value of v for the portion of a sample (near the surface) from which most of the diffraction occurs is not easy to determine. For use with these samples, an approximate value of $v=0{\cdot}36$ was obtained from measurements on packed

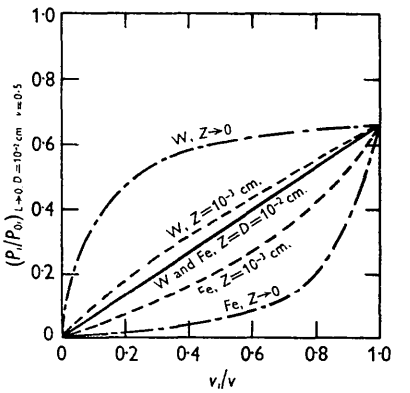

Fig. 10. Effect of grain size on power diffracted from an iron–tungsten mixture. Grain size is the same for both components, and Fe $K\alpha$ radiation is considered.

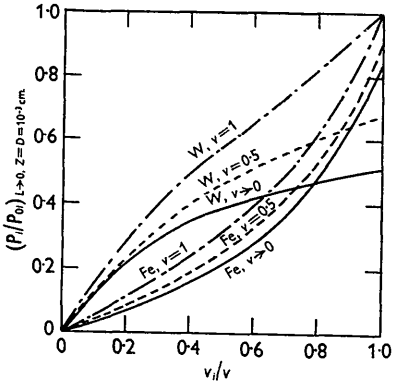

Fig. 11. Effect of degree of compaction on power diffracted from an iron–tungsten mixture. The absorption effects were evaluated for Fe $K\alpha$ radiation.

iron powder; an attempt was made to achieve the same degree of compaction as in sample preparation.

Crystal diameters, assuming spherical crystals of uniform size, were measured by Patterson's (1936) equation,

$$L=1{\cdot}1\lambda/(B\cos\theta). \tag{29}$$

The quantity B is the line broadening attributable to crystal size and was determined from the measured line breadth B_m for the sample by

$$B^2=B_m^2-B_0^2, \tag{30}$$

B_0 being the line breadth for a sample in which the crystals are sufficiently large so that crystal-size line broadening is negligible (Warren, 1938*a*).

Particle diameters were measured with the aid of a microscope. In order to make use of the equation derived for powders consisting of particles of uniform size, an effective diameter, D, was obtained by means of the average

$$D=\sum_n D_n^3/\sum_n D_n^2, \qquad (31)$$

where D_n is the diameter of the nth particle.*

The linear absorption coefficients used (573 cm.$^{-1}$ for Fe and 6170 cm.$^{-1}$ for W) are based on values in the *International Tables...* (1944, vol. 2), and ϵ (4570 cm.$^{-1}$ for Fe) was computed by equations (16) and (17).

Effect of particle size; single substance

Description of the sample materials used in this and in following experiments are given in Table 1, and particle-size distributions are shown as cumulative plots in Fig. 12.

Table 1. *Descriptions of sample materials*

Designation	Source of material, preparation, etc.	D, average particle diameter (cm.)
A	Carbonyl iron from General Aniline Works. GAF Type C	$4{\cdot}9\times10^{-4}$
B	Carbonyl iron from General Aniline Works. GAW Type C	7·3
C	Baker's iron powder by hydrogen. As received, all the powder passed through No. 325 standard sieve (0·0044 cm.). Particle size analysis by weight: 7 % material *D*, 21 % *E* and 72 % *F*	23·5
D	Nominal 0 to 0·0010 cm. cut of *C*, obtained by air elutriation	10·8
E	Nominal 0·0010 to 0·0020 cm. cut of *C*	14·2
F	Nominal 0·0020 to 0·0044 cm. cut of *C*	33·9
G	Iron microspheres, prepared by spraying molten metal. Reduced in hydrogen atmosphere	20·7
H	Armco iron, sawdust prepared from a solid metal casting. Sifted through No. 200 sieve and remaining on No. 325 sieve	56·2
I	Armco iron sawdust, through No. 180 and on No. 200 sieves	79†
J	Armco iron sawdust, on No. 100 sieve	290
K	Tungsten powder by hydrogen reduction, from North American Philips	5·4

† Average of the nominal openings for the two sieves used.

Experimental and theoretical results for the effect of particle size on integrated intensity are compared in Table 2. Tentatively, the values $\alpha=\beta=0$ were considered in equation (15). Slight corrections for crystal size were made to the measured relative integrated intensities, and the corrected value for sample *B* was adjusted to coincide with its theoretical value of $(P/P_0)_{L\to0}$. The remaining integrated intensities (corrected for crystal size) were then scaled relative to that of sample *B*; these are the experimental values of $(P/P_0)_{L\to0}$ in Table 2.

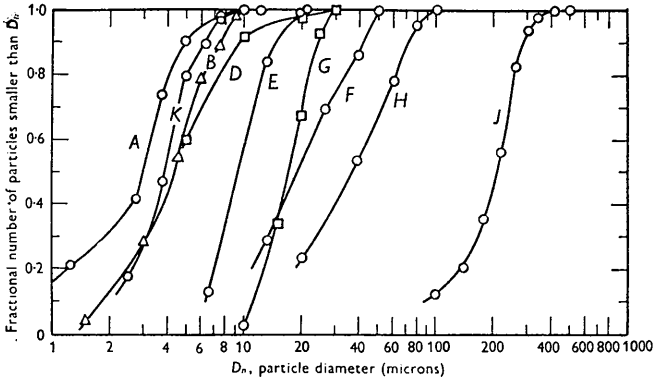

Fig. 12. Cumulative particle-size plots, obtained by microscope count. Letters correspond to samples in Table 1.

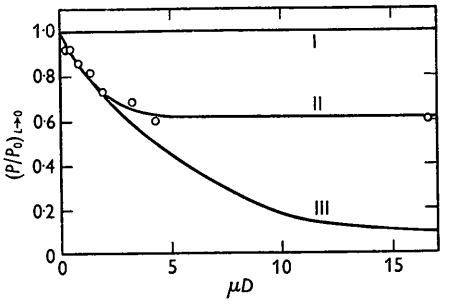

Fig. 13. Comparison of experiment with several theories for the effect of powder coarseness on the power diffracted from a sample of a single substance. The points are experimental; curve I (no effect) is according to Brindley's theory; curve II is for the present theory; curve III is for the theoretical equation derived by de Wolff.

Table 2. *Particle-size effect; single substance. Comparison of experiment with theory for iron powders*

For all samples $v=0{\cdot}36$ (estimate)

Sample material	Relative integrated intensity	μD	L (A.)	$(P/P_0)_{L\to0}$ Exp.	$(P/P_0)_{L\to0}$ Theor.
A	0·99	0·28	1200	0·92	0·94
B	1·00	0·43	825	0·92	0·92
E	0·93	0·81	430	0·86	0·85
C	0·89	1·35	490	0·82	0·79
F	0·80	1·98	490	0·73	0·73
H	0·75	3·22	360	0·69	0·66
I	0·65	4·30	420	0·60	0·63
J	0·66	16·6	490	0·61	0·61

In Fig. 13, graphical comparisons are made of the experimental results with several theories. Brindley's theory, predicting integrated intensity independent of particle size, is definitely not in accord with the data. The curve for de Wolff's theory was constructed from

* The choice of this average was based on the following considerations. Values of P/P_0 were computed directly for a number of two-sized particle distributions in laminar models for which $\mu Y_n\leqslant2$, the size ratio of large to small particles is between 1 and 5, and $v=0{\cdot}36$ and 0·50. These power ratios were compared with the values obtained by using equation (12) in which Y was computed by averages of the form $\sum_n Y_n^x/\sum_n Y_n^{x-1}$, where $x=1$, 2, 3 and 4. Results for $x=3$ were generally most satisfactory; the values of P/P_0 thus obtained departed from the directly computed values by less than 3 % in all the cases.

the appropriate equation in his paper. In the present notation, this equation is

$$P/P_0 = \exp\{-\tfrac{1}{2}\mu(\tfrac{2}{3}D)(1-v)^2\}. \quad (32)$$

For values of $\mu D < 2$, this equation fits the experimental data very well, but predicts too low values for larger μD. The present theory fits the experimental points throughout the entire range of μD tested, indicating that the form of the particle factor is essentially correct and that $\alpha = 0$ is a satisfactory choice for these samples. The data also indicate that the effective average particle size given by (31) gives satisfactory results, even in the case of a rather wide particle size distribution such as found in sample material *C*.

Effect of degree of compaction; single substance

A variation in the degree of compaction was obtained by varying the proportion of the components in a suspension of iron in bees wax. A portion of iron microspheres (material *G* in Table 1) was completely immersed in about its own volume of molten wax. As the mixture cooled to a state of high viscosity, settling of the iron was prevented by stirring. Because of the spherical form of the particles, the sample was free from preferred orientation. The integrated intensity, P_{I}, for this sample was measured in arbitrary units. For a similar sample, with about three times as much wax as iron, the integrated intensity P_{II} was measured. Equation (19), with $\alpha = 0$, was used for obtaining the theoretical ratio $P_{\mathrm{II}}/P_{\mathrm{I}}$. Results of this study are summarized in Table 3. Agreement between the theoretical ratio 0·87 and the experimental ratio 0·85 is considered very satisfactory. However, it is of interest to note that if the theory for ideal powders were used instead of equation (19), the calculated ratio turns out to be 0·96, definitely not in agreement with the experiment.

Table 3. *Effect of degree of compaction in a single substance. Comparison of experiment with theory*

Material: powder *G*, Table 1; $\mu D = 1{\cdot}19$
Composition of wax: 80·2 % C, 6·3 % O, 13·5 % H
Density of wax: 0·96 g.cm.$^{-3}$
Linear absorption coefficient of wax = 9·84 cm.$^{-1}$
Sample I: $v_{\mathrm{Fe}} = 0{\cdot}478$, $v_{\mathrm{wax}} = 0{\cdot}552$
Sample II: $v_{\mathrm{Fe}} = 0{\cdot}232$, $v_{\mathrm{wax}} = 0{\cdot}768$
Experimental $P_{\mathrm{II}}/P_{\mathrm{I}} = 0{\cdot}85$
Theoretical $P_{\mathrm{II}}/P_{\mathrm{I}} = 0{\cdot}87$

Particle-size effect in mixed powder

The effect of particle size was investigated for a simple iron–tungsten mixture in which the particle size in both components was approximately the same. Integrated intensities $P_{\mathrm{Fe\,mix.}}$ and $P_{\mathrm{W\,mix.}}$ for the components in the mixture were compared respectively with the integrated intensities $P_{\mathrm{Fe\,alone}}$ and $P_{\mathrm{W\,alone}}$ for samples of these components by themselves. Corresponding theoretical values were obtained by equations (27) and (15). The agreement between theoretical and experimental values of $P_{i\,\mathrm{mix.}}/P_{i\,\mathrm{alone}}$ is rather good. If, however, the mixture were treated as an ideal powder, the computed values are 0·096 for iron and 0·904 for tungsten. These values differ substantially from the respective experimental ratios 0·22 and 0·74, and serve to emphasize that the particle-size effect may be serious even for apparently fine powders, the particle size being only five microns in this case.

Table 4. *Particle-size effect; mixed powder. Comparison of experiment with theory*

All samples: $v = 0{\cdot}36$ (estimate)
Iron: powder *A*, Table 1; $\mu D_{\mathrm{Fe}} = 0{\cdot}28$
Tungsten: powder *K*, Table 1; $\mu D_{\mathrm{W}} = 3{\cdot}27$
Mixture: $v_{\mathrm{Fe}} = 0{\cdot}192$, $v_{\mathrm{W}} = 0{\cdot}168$, $D \sim 5{\cdot}1 \times 10^{-4}$ cm.
$\mu D_{\mathrm{Fe}} = 0{\cdot}29$, $\mu D_{\mathrm{W}} = 3{\cdot}14$

$\dfrac{P_{\mathrm{Fe\,mix.}}}{P_{\mathrm{Fe\,alone}}} = 0{\cdot}22$, experimental
$= 0{\cdot}22$, theoretical

$\dfrac{P_{\mathrm{W\,mix.}}}{P_{\mathrm{W\,alone}}} = 0{\cdot}74$, experimental
$= 0{\cdot}75$, theoretical

Effect of crystal size

Samples were prepared from iron powder *B*, Table 1, and heated at elevated temperatures to induce various degrees of crystal growth. It was found convenient to prepare each sample by pressing the powder into a shallow well machined in an iron plate whose dimensions in inches are roughly $1 \times \frac{3}{4} \times \frac{1}{8}$. The flat powder block could then be heat-treated without disturbing the arrangement of the particles. Several such samples were made up and treated in a hydrogen atmosphere for the durations and approximate temperatures given in Table 5.

From line-broadening measurements, the crystal sizes were computed and the crystal factors calculated therefrom by (15). The value of the integrated intensity for the untreated sample was then adjusted to equal the value computed from line-broadening measurements. Integrated intensities for the other samples were then measured relative to this adjusted value for the

Table 5. *Effect of crystal size in iron powder*

Heat treatment of sample	Relative integrated intensity	Line breadth (°)		Quantities from power measurements		Quantities from line-broadening measurements	
		B_m	B_0	$(P/P_0)_{D\to 0}$	L (A.)	$(P/P_0)_{D\to 0}$	L (A.)
Untreated	1·00	0·267	0·230	0·97	825	0·97	825
40 min. at 900° F.	0·98	0·260	0·235	0·95	1,600	0·96	1,240
10 min. at 1000° F.	0·97	0·275	0·240	0·94	1,700	0·96	1,030
60 min. at 900° F.	0·88	0·263	0·238	0·86	6,000	0·93	1,600
80 min. at 900° F.	0·79	0·250	0·225	0·77	10,000	0·93	1,600
15 min. at 1500° F.	0·65	0·237	0·230	0·64	20,000	0·92	2,500
2 hr. at 1500° F.	0·50	0·230	0·230	0·49	33,000	—	—

untreated sample; these are the measured values of $(P/P_0)_{D\to 0}$. Values of crystal size were also computed from the measured crystal factors. These data are summarized in Table 5. It will be observed that, qualitatively, the expected trend obtains, i.e. with increasing severity of heat treatment, the crystal size increases and the diffracted power decreases. However, wherever a comparison could be made, the measured values of diffracted power are seen to be consistently smaller than the corresponding values computed from crystal-size measurements. Since the equations involved have been derived for crystals of uniform size, it might be suspected that the cause for the discrepancy might be due to a non-adherence to this requirement of crystal-size uniformity. Indeed, the nature of the discrepancy is such that it can be accounted for on the basis of the presence of crystal-size distributions. For instance, if a diffraction peak is approximated by a Gaussian error curve (Warren, 1938*b*), then, under the experimental conditions employed, a mixture by weight of 4 % of 600 A., 89 % of 1240 A., and 7 % of 5000 A. crystals will produce a line broadening corresponding to a crystal size 1240 A., and will have a value 0·95 for $(P/P_0)_{D\to 0}$; these are the experimental values for the sample treated 40 min. at 900° F. Furthermore, it can be shown that under the experimental conditions employed, this simple mixture will also give the same peak height and will approximate the shape of the observed curve rather well. The other cases can be similarly reconciled by appropriately chosen crystal-size distributions. Although the observed results can thus be rationalized, the present experiment is somewhat inconclusive owing to the lack of accurate information on the crystal-size distributions.

Discussion and conclusions

In cases where favorable experimental conditions were realized, the theory presented was satisfactorily confirmed. Although further experimental tests are desirable, the results so far indicate that the theory can be useful in the accurate measurement of integrated intensities. For instance, it can be used to ascertain whether, within the allowable experimental error, a sample can be treated as an ideal or non-ideal powder. In the latter case the theory can be helpful in evaluating the diffraction results. These considerations can be significant even for powders that might not ordinarily be considered coarse with respect to crystal, grain, or particle size.

The fact that the state of subdivision of the sample material can modify the magnitude of the diffracted power suggests that power measurements might be used in special cases to determine effective average sizes of crystals, grains and particles. It will be observed that in the case of iron and tungsten, the suggested power-measurement method for determining crystal size begins to become sensitive at approximately the upper limit of practicability of the line-broadening method, the useful range for the power method being about 10^{-5} to 10^{-3} cm.

Although the discussion was concerned chiefly with crystalline powders, the results are also applicable in part to solid blocks of polycrystalline materials and to amorphous powders.

The writer is pleased to express his appreciation to Mr J. S. McIlhenny for the determinations of the particle-size distributions by microscope count.

References

Brentano, J. C. M. (1935). *Proc. Phys. Soc. Lond.* **47**, 932.

Brentano, J. C. M. (1938). *Proc. Phys. Soc. Lond.* **50**, 247.

Brindley, G. W. (1945). *Phil. Mag.* **36**, 347.

Compton, A. H. & Allison, S. K. (1946). *X-Rays in Theory and Experiment*. New York: Van Nostrand.

Darwin, C. G. (1914). *Phil. Mag.* **27**, 675.

Friedman, H. (1945). *Electronics*, **18**, 132.

Havinghurst, R. J. (1926). *Phys. Rev.* **28**, 882.

International Tables for the Determination of Crystal Structures (1944). Ann Arbor: Edwards.

Patterson, A. L. (1936). *Phys. Rev.* **49**, 884.

Prins, J. A. (1930). *Z. Phys.* **63**, 477.

Rusterholz, A. (1931). *Helv. phys. Acta*, **4**, 68.

Schäfer, K. (1933). *Z. Phys.* **86**, 738.

Taylor, A. (1944*a*). *Phil. Mag.* **35**, 218.

Taylor, A. (1944*b*). *Phil. Mag.* **35**, 404.

Warren, B. E. (1938*a*). *J. Amer. Ceram. Soc.* **21**, 49.

Warren, B. E. (1938*b*). *Z. Krystallogr.* **99**, 448.

Wolff, P. M. de (1947). *Physica, 's Grav.*, **13**, 62.